

Revealing half-metallicity: Predicting large bandgaps in halogen-based full-Heusler alloys

Iltaf Muhammad^{a,b}, Shehzad Ahmed^a, Naeem Ullah^a, Muhammad Mushtaq^d, Maryam Liaqat^e, Xiaoqing Tian^{a,c,*}, Jian-Min Zhang^b

^a College of Physics and Optoelectronic Engineering, Shenzhen University, Shenzhen 518060, China

^b College of Physics and Information Technology, Shaanxi Normal University, Xian 710119, Shaanxi, China

^c International Center for Quantum Materials, School of Physics, Peking University, Beijing 100871, China

^d Department of Physics, University of the Poonch Rawalakot, Rawalakot 12350, AJK, Pakistan

^e Department of Computational Physics, University of Okara, Okara, Pakistan

ARTICLE INFO

Keywords:

Heusler alloys
Electronic structures
Magnetic properties
Thermoelectric properties
First-principles

ABSTRACT

As for spintronic applications, all information is encoded in the spin degree of freedom, so the key issues are the high spin-polarization, large half-metallic (HM) bandgap, large magnetic moment and higher Curie temperature than room temperature. In this paper, we studied halogen based CsYZ_2 ($\text{Y} = \text{V}$ or Cr ; $\text{Z} = \text{F}$, Cl , Br or I) full-Heusler alloys. Our study reveals that CsVF_2 , CsVCl_2 , CsVI_2 and CsCrI_2 alloys are all HM ferromagnets while remaining alloys exhibits magnetic semiconductor behavior. The electronic structures indicate that these alloys open very large bandgaps in the spin-down channel. Following the Slater-Pauling rule $M_t = Z_t - 16$, these alloys exhibit very large total magnetic moments M_t of $4.00 \frac{\mu_B}{f.u.}$ when $\text{Y} = \text{V}$ and $5.00 \frac{\mu_B}{f.u.}$ when $\text{Y} = \text{Cr}$. The high Curie temperatures indicate these alloys are appropriate for spintronic applications at room temperature. Furthermore, the absorption coefficient $\alpha(\omega)$ of the CsVF_2 alloy is better from other alloys in the visible region. The maximum $ZT = 0.7$ is obtained for CsCrBr_2 and is an ideal candidate for thermoelectric (TE) applications.

Introduction

In spintronics [1–4], also known as spin electronics, not only charge of the electron is used, but the spin and magnetic moment of the electron are also used. The spintronic devices not only transport the charge, but also use the spin and magnetic moment of the electron. The hard disk heads, magnetic random memory, spin field emission transistors, spin light-emitting diodes are all potential applications of spintronics. In the emerging fields of internet and big data, the spin random storage based on spin electronics has become an excellent candidate device due to its low storage power consumption. However, in order to reduce the storage power consumption of spintronic devices, it is necessary to increase the injection rate of spin electrons. If spin electrons are injected into semiconductors from traditional ferromagnetic materials, the efficiency is very low. On the other hand, the electron spin-polarization of traditional ferromagnetic materials is low, also, the resistivity of semiconductors is large because of the small resistivity of ferromagnetic materials, and the resistivity of the two does not match. Therefore, it is one of the most important topics for researchers to explore new

materials for spintronic devices. In recent years, magnetic semiconductors, spin-gapless semiconductors, half-metals and other new materials have attracted more and more researcher's attention, while half-metallic (HM) materials have attracted more and more attention because of its special band structure. At the Fermi level E_F , one spin channel of the electron shows metallic behavior, while the other spin channel show semiconductor behavior, so it has 100 % spin-polarization at the Fermi level E_F , becoming one of the most ideal spin electron injection source materials, making HM materials possible in the application of spintronics. As a kind of HM material with 100 % SP, Heusler alloy has naturally become a favorite in the field of spintronics.

In 1903, German scientist Friedrich Heusler [5] found that by adding Al element to Cu and Mn transition metal (TM) elements, a Cu_2MnAl alloy was obtained which showed an adjustable magnetism while all the atoms in the alloy were non-magnetic (NM). De Groot *et al.* [6] discovered ferromagnetic behavior in NiMnSb half-Heusler alloy, after that the other group III-V sp-elements (Z) were also added with TM elements (XY) and obtained other Heusler alloys. Many researchers explored the electronic, optical, thermoelectric, mechanical, surface,

* Corresponding author at: College of Physics and Optoelectronic Engineering, Shenzhen University, Shenzhen 518060, China.

E-mail address: xqtian@szu.edu.cn (X. Tian).

dynamic and catalytic properties of the Heusler alloys [7–13]. From point view of compositions, the Heusler alloys can be divided into ternary (half- and full-Heusler) [14–18] and quaternary Heusler alloys [19]. The half-Heusler alloys have the chemical formula XYZ, where X and Y are transition-metal elements while Z is *sp* elements. Usually, half-Heusler alloys crystallize in the *C1_b*-type crystal structure with space group *F*₄*3**m* (No. 216). Similarly, the full-Heusler alloys have the chemical formula X₂YZ and crystallize in two types of structures, *i.e.* the Cu₂MnAl-type structure and the Hg₂CuTi-type structure. In Cu₂MnAl-type structure, the X atoms are located at 4a (0, 0, 0) and 4d (3/4, 3/4, 3/4), Y at 4b (1/2, 1/2, 1/2), Z at 8c (1/4, 1/4, 1/4) Wyckoff positions in the unit cell of space group Fm₃*m* (No. 225). While in Hg₂CuTi-type structure, the X atoms are located at 4d (3/4, 3/4, 3/4), Y at 4b (1/2, 1/2, 1/2), Z at 4a (0, 0, 0) and 4c (1/4, 1/4, 1/4) Wyckoff positions in the unit cell of space group *F*₄*3**m* (No. 216) [20]. When one of the X atom is replaced by an alternate transition-metal element X', quaternary Heusler alloy XX'YZ with a space group *F*₄*3**m* (No. 216) is obtained, which is known as LiMgPdSn type structure. Similarly, binary Heusler alloys XZ, X₂Z and X₃Z can be obtained by substituting or vacancy in ternary half-Heusler alloy XYZ and full-Heusler alloy X₂YZ. Specifically, (1) if we leave the Y atom vacant, the ternary half-Heusler alloy XYZ will become the binary Heusler alloy XZ. (2) If we replace the X atom with the Y atom, the ternary half-Heusler alloy XYZ will become the binary Heusler alloy X₂Z. (3) If we let the Y atom vacancy in X₂YZ, it will become a binary Heusler alloy X₂Z [21]. (4) If we replace the Y atom with the X atom in X₂YZ, it will become a binary Heusler alloy X₃Z [22,23].

Recently, many researchers added groups IA, IIA and VIA with TM elements and obtained Heusler alloys with large magnetic moments, complete 100 % spin-polarization and large HM bandgaps. Fan *et al.* [24] studied the magnetism and HM character of the CsYO₂ (Y = V, Cr, Mn, Fe, Co or Ni) Heusler alloys and found that these alloys had large HM bandgaps and their magnetic moments were 2, 3, 4, 5, 4 or 3 $\frac{\mu_B}{f.u.}$, respectively. Wang *et al.* [25] found the magnetic moment of XCrZ (X = Li, K, Rb or Cs; Z = S, Se or Te) half-Heusler alloys could reach to 5 $\frac{\mu_B}{f.u.}$. Cherid *et al.* [26] found the magnetic moment of the Cs₂CrGe full-Heusler alloy was 4 $\frac{\mu_B}{f.u.}$. Damewood *et al.* [27] found the magnetic moments of the LiMnZ (Z = N, P or Si) half-Heusler alloys were 4 $\frac{\mu_B}{f.u.}$ when Z = Si and 5 $\frac{\mu_B}{f.u.}$ when Z = N and P. In these alloys, the origin of half-metallicity is attributed to the p-d hybridization between sp-elements and TM elements. More recently, the first-principles study of Song *et al.* [22] showed that the ZCl₃ (Z = Be, Mg, Ca or Sr) binary Heusler alloys without TM elements are HM with total magnetic moment of 1 $\frac{\mu_B}{f.u.}$.

Because of their potential for ground-breaking applications in spintronics, magneto-optics, and energy conversion, studies of the electronic structure, magnetic behavior, optical response, and thermoelectric performance of halogen-based Heusler alloys are important. Accordingly, our specific goals are to investigate optical features, analyze the thermoelectric potential of these alloys, and assess the impact of halogen atoms on the electronic band structure and magnetic ordering events. We make use of recent advancements in the field to place our work in the perspective of the present research environment. Distinguished sources, including [28–34], have furnished significant perspectives on the electrical and magnetic characteristics of Heusler alloys, establishing the foundation for our inquiry. These studies emphasize the importance of comprehending the basic properties of Heusler materials as well as their possible technological ramifications. Our work expands and improves upon these initial investigations by providing a more detailed look at how halogen atoms influence the characteristics of the material.

In this paper, we investigate the structural, electronic, magnetic and optical properties of the halogen based full-Heusler alloys CsYZ₂ (Y = V or Cr; Z = F, Cl, Br or I). The paper is organized as follows: Section 2 is comprised of the methodology and computational details which we have used in this paper. In section 3, we have incorporated all the theoretical aspects of the structural, electronic, magnetic, optical and

thermoelectric properties of these alloys by using GGA and HSE06 methods. Finally, in the last section, we summarize our results and outcomes. The computational simulation is a promising tool for predicting the novel materials and properties. So, our prediction about the large HM bandgaps and large magnetic moments of the CsYZ₂ (Y = V or Cr; Z = F, Cl, Br or I) full-Heusler alloys needs to be verified through experimental studies.

Method of calculations

First-principle calculations based on the density functional theory (DFT) [35–38] using Vienna ab-initio simulation package (VASP) are performed to compute the structural, electronic, magnetic and optical properties of the CsYZ₂ (Y = V or Cr; Z = F, Cl, Br or I) full-Heusler alloys. The projector augmented wave (PAW) method [39] is used to treat the interaction between the atomic core and the valence electrons. The generalized gradient approximation (GGA) within the framework of Perdew-Burke-Ernzerhof (PBE) [40] is used to describe electronic exchange and correlation. We also used the HSE06 functional [41] to obtain more accurate electronic structure. A k-point mesh of 9 × 9 × 9 is used for the sampling of the k-space together with a Gaussian smearing broadening of 0.05 eV. The cut-off energy is chosen to be 500 eV for the plane-wave basis set. The tolerance parameter for the self-consistent loops is chosen to be 10⁻⁶ eV and the ions are fully relaxed until the maximum Hellmann-Feynman forces are less than 0.02 eV/Å. The Cs (6 s¹), V (3d³4s²), Cr (3d⁵4s¹), F (2s²2p⁵), Cl (3s²3p⁵), Br (4s²4p⁵) and I (5s²5p⁵) electrons are treated as valence electrons.

Results and discussions

Structural properties

The Cu₂MnAl-type and Hg₂CuTi-type structures of the CsYZ₂ (Y = V or Cr; Z = F, Cl, Br or I) full-Heusler alloys are shown in Fig. 1 (a) and (b). In Cu₂MnAl-type structure, the Cs atoms are located at 4a (0, 0, 0), Y at 4b (1/2, 1/2, 1/2), Z at 8c (1/4, 1/4, 1/4) Wyckoff positions in the unit cell of space group Fm₃*m* (No. 225). While in Hg₂CuTi-type structure, the Cs atoms are located at 4d (3/4, 3/4, 3/4), Y at 4b (1/2, 1/2, 1/2), Z at 4a (0, 0, 0) and 4c (1/4, 1/4, 1/4) Wyckoff positions in the unit cell of space group *F*₄*3**m* (No. 216).

To find the most stable magnetic state and crystal structure of the CsYZ₂ (Y = V or Cr; Z = F, Cl, Br or I) full-Heusler alloys, the structure optimization is carried out firstly in the ferromagnetic (FM), anti-ferromagnetic (AFM) and NM states for the Cu₂MnAl-type and Hg₂CuTi-type structures. The optimized lattice constants a₀ and total energies E_t in FM, AFM and NM states of the CsYZ₂ (Y = V or Cr; Z = F, Cl, Br or I) full-Heusler alloys in Cu₂MnAl-type and Hg₂CuTi-type structures are listed in Table S1. It is found that the Cu₂MnAl-type structure is the most stable structure in the FM state due to the lowest total energies of -71.04, -60.71, -56.85, -52.38, -76.46, -66.06, -62.19 and -57.66 eV at optimized lattice constants of 6.71, 7.67, 8.00, 8.45, 6.75, 7.73, 8.05 and 8.52 Å for CsVF₂, CsVCl₂, CsVBr₂, CsVI₂, CsCrF₂, CsCrCl₂, CsCrBr₂ and CsCrI₂, respectively. Fig. 1 (c) show the total energy as a function of lattice constant for CsYZ₂ (Y = V or Cr; Z = F, Cl, Br or I) full-Heusler alloys in FM phase. This shows that the total energy of FM phase is ground state energy and there is no metastable state. The optimized lattice constants vary according to the variation of atomic radius of halogen-atoms as 0.42 (F) < 0.79 (Cl) < 0.94 (Br) < 1.15 (I) Å [42] for either Y = V or Cr cases. Our results also show that the CsCrF₂ is the most stable material due to lowest total energy. Therefore, we only further consider the CsYZ₂ (Y = V or Cr; Z = F, Cl, Br or I) full-Heusler alloys with Cu₂MnAl-type structure in FM state.

To our knowledge, the CsYZ₂ (Y = V or Cr; Z = F, Cl, Br or I) full-Heusler alloys have not been previously investigated theoretically or experimentally. Therefore, we study the cohesive energy E_c as a basis for

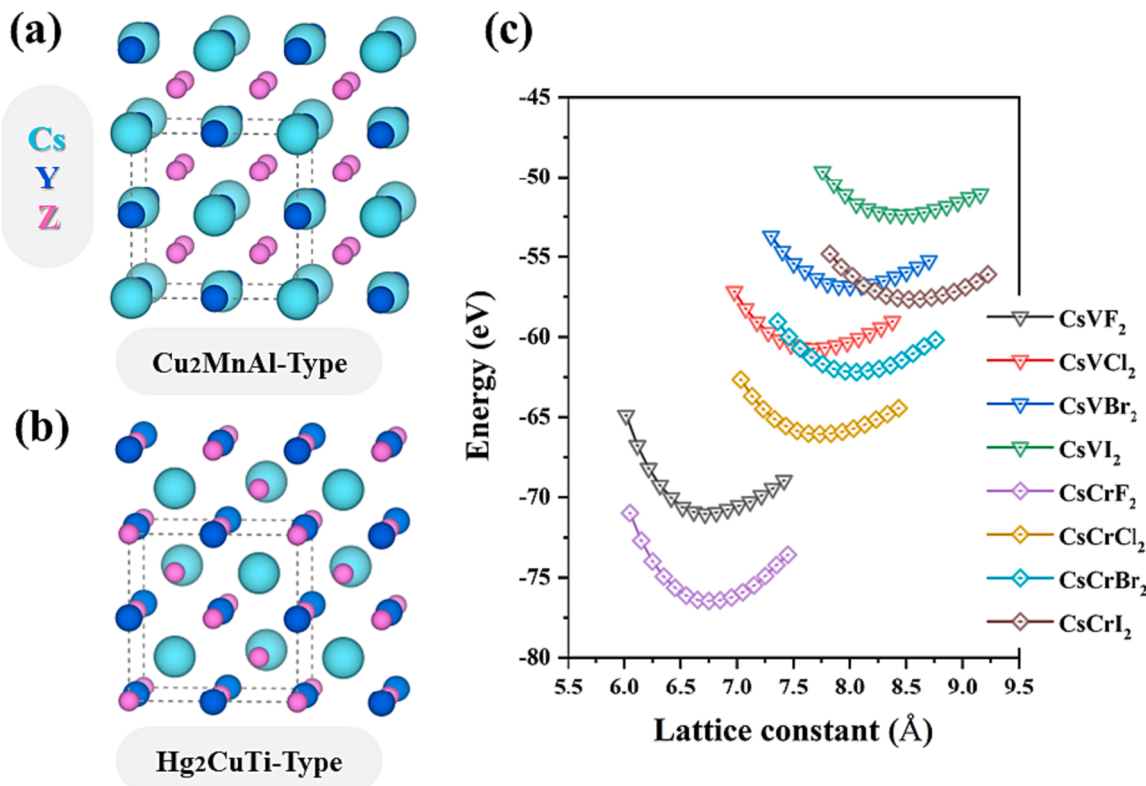


Fig. 1. The (a) Cu₂MnAl-type, (b) Hg₂CuTi-type crystal structures and (c) total energy as a function of lattice constant for CsYZ₂ (Y = V or Cr; Z = F, Cl, Br or I) full-Heusler alloys in FM phase.

studying their structural stability. The cohesive energy E_c is calculated by:

$$E_c = E_{\text{Cs}}^{\text{iso}} + E_Y^{\text{iso}} + 2E_Z^{\text{iso}} - E_t \quad (1)$$

where $E_{\text{Cs}}^{\text{iso}}$, E_Y^{iso} , E_Z^{iso} denote the chemical potential of the isolated components Cs, Y, Z (Y = V or Cr; Z = F, Cl, Br or I), E_t is the optimized total energy of each alloy per formula unit. Table S2 shows that the high cohesive energies signify these eight alloys are stable. For either Y = V or Cr cases, the cohesive energies vary according to the variation of the electronegativities of halogen-atoms as 3.98 (F) > 3.16 (Cl) > 2.96 (Br) > 2.66 (I) [43].

The formation energy E_f of the CsYZ₂ (Y = V or Cr; Z = F, Cl, Br or I) full-Heusler alloys is calculated by:

$$E_f = E_t - (E_{\text{Cs}}^{\text{bulk}} + E_Y^{\text{bulk}} + 2E_Z^{\text{bulk}}) \quad (2)$$

where E_t represents the total energy of each alloy per formula unit, $E_{\text{Cs}}^{\text{bulk}}$, E_Y^{bulk} and E_Z^{bulk} represent the energies of each atom in bulk Cs, Y and Z (Y = V or Cr; Z = F, Cl, Br or I), respectively, (bulk Cs, Cr or V with body-centered cubic structure, F with base-centered monoclinic structure, Cl, Br or I with base orthorhombic structure). As listed in Table S2, the negative formation energies indicate the formation processes of these eight alloys are exothermic and thus easily to be synthesized in experiments. For either Y = V or Cr cases, the absolute values of the formation energies vary according to the variation of the electronegativities of halogen-atoms as 3.98 (F) > 3.16 (Cl) > 2.96 (Br) > 2.66 (I) [43]. Both the cohesive energies and formation energies ensure the thermodynamical stability of the CsYZ₂ (Y = V or Cr; Z = F, Cl, Br or I) full-Heusler alloys.

The value of Curie Temperature (T_C) determines whether a magnetic material is suitable for room temperature (RT) applications. If a magnetic material's T_C falls below RT, it loses its magnetic property and is thus inappropriate for applications. T_C is an important parameter for

spintronics and magnetoelectronics that can be determined using mean field approximation. In the mean field approximation, the Curie temperature can be described by the standard statistical method in the nearest Heisenberg model. The T_C can be calculated directly from the energy difference (ΔE) between the AFM and FM phases as follows [44,45]:

$$T_C = \frac{2\Delta E}{3k_B} \quad (3)$$

where, k_B is the Boltzmann constant. The estimated values are listed in Table S2. The higher T_C indicate that these eight alloys are appropriate for spintronic applications at room temperature. Our results are in comparable with the results of the T_C for other Heusler alloys calculated by mean field approximation as for Co₂FeAl and Fe₂CoAl full-Heusler alloys are 1332.2 K and 1025.4 K, respectively [46]. The importance of determining T_C using mean field approximation stems from its capacity to predict the onset of magnetic phase transitions and provide information about the temperature range throughout which ferromagnetic order is maintained. This knowledge is invaluable for understanding materials' magnetic behavior and predicting their performance under different heat conditions. Furthermore, T_C is an important parameter in the design and optimization of magnetic materials for technical applications such as magnetic data storage devices, magnetic sensors, and spintronics.

Electronic properties

First, we analyze the spin-polarized band structures of the CsYZ₂ (Y = V or Cr; Z = F, Cl, Br or I) full-Heusler alloys are shown in Fig. 2 by HSE06 method and in Fig. S1 by GGA method. The Fermi level E_F is set at zero energy and indicated by the horizontal black lines. The red and blue lines represent the spin-up and spin-down channels, respectively. In GGA method, the band structures show that for all alloys, the spin-up

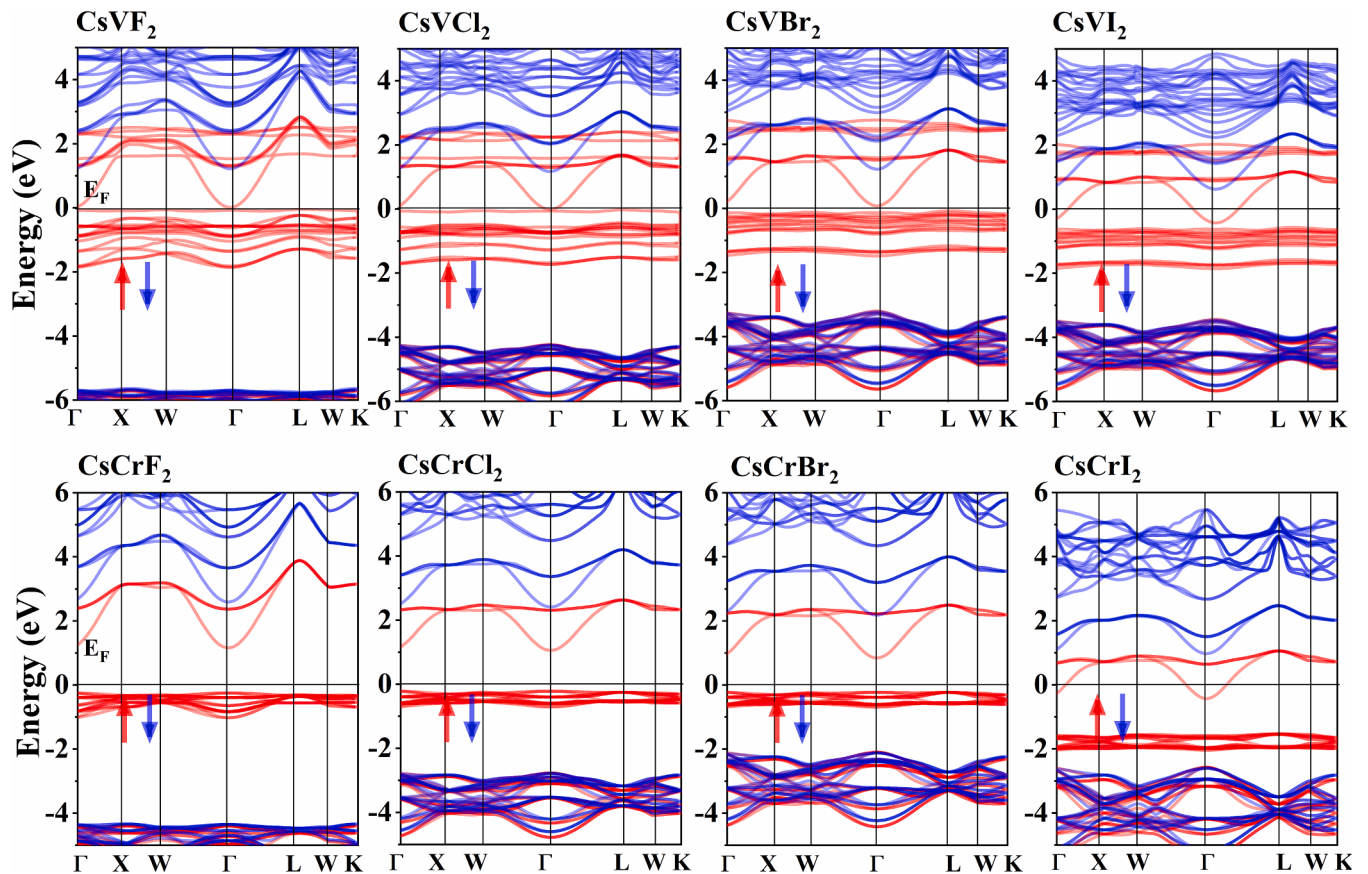


Fig. 2. The spin-polarized band structures of the CsYZ_2 ($Y = \text{V}$ or Cr ; $Z = \text{F}$, Cl , Br or I) full-Heusler alloys using HSE06 method.

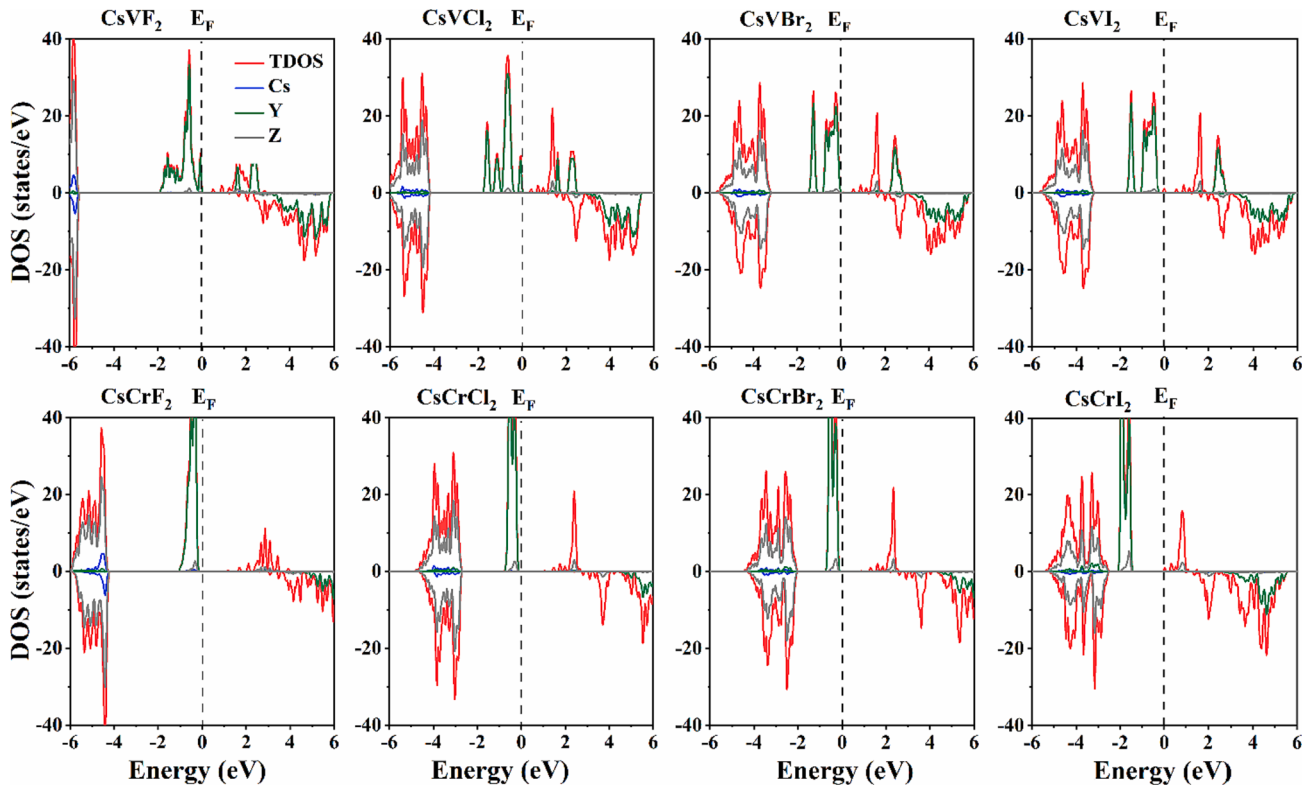


Fig. 3. The total density of states (TDOS) and atom-projected density of states (APDOS) of the CsYZ_2 ($Y = \text{V}$ or Cr ; $Z = \text{F}$, Cl , Br or I) full-Heusler alloys using HSE06 method.

channels cross the Fermi level E_F , while the spin-down channels open the bandgaps at the Fermi level E_F . The bandgap in one of the two spin channels confirms that these alloys are HM. While in HSE06 calculations, the spin-up channels in the CsVF₂, CsVCl₂, CsVI₂ and CsCrI₂ alloys cross the Fermi level E_F , the CsVBr₂ open a small bandgap of 0.190 eV at the Fermi level E_F , while the CsCrF₂, CsCrCl₂ and CsVBr₂ alloys have bandgaps of 1.403, 1.268 and 1.072 eV, respectively. while the spin-down channels open large bandgaps at the Fermi level E_F . Thus, the the CsVF₂, CsVCl₂, CsVI₂ and CsCrI₂ alloys are HM ferromagnets while the CsVBr₂, CsCrF₂, CsCrCl₂ and CsVBr₂ alloys are magnetic semiconductors (MSC). The values of the spin-up bandgap $E_{g\uparrow}$ (eV), spin-down bandgap $E_{g\downarrow}$ (eV) and electronic properties in the spin-up and spin-down channels of the CsYZ₂ ($Y = V$ or Cr; $Z = F$, Cl, Br or I) full-Heusler alloys are listed in Table S3 by GGA method and in Table S4 by HSE06 method. Also, the spin-down bandgap $E_{g\downarrow}$ of the CsYO₂ ($Y = V$ or Cr) alloys [24] are given for comparison. It can be seen that, in spin-down channel the VBM shifts upwards to high energy for halogens from F to I, but the CBM does not move significantly, which lead to a decrease in the spin-down bandgap $E_{g\downarrow}$ of 4.92, 4.07, 3.29 and 2.73 eV for $Y = V$ case and 4.59, 3.81, 3.08 and 2.54 eV for $Y = Cr$ case by GGA method. While by HSE06 calculations, the same variation is found in the spin-down channel and the noted values of spin-down bandgap $E_{g\downarrow}$ of 6.895, 5.523, 4.421 and 4.320 eV for $Y = V$ case and 6.937, 5.192, 4.299 and 3.535 eV for $Y = Cr$ case is obtained. Our results show that the CsVF₂ alloy has the most stable HM electronic structure due to the large spin-down bandgap $E_{g\downarrow}$.

In more detail, the total density of states (TDOS) and atom-projected density of states (APDOS) of the CsYZ₂ ($Y = V$ or Cr; $Z = F$, Cl, Br or I) full-Heusler alloys in Fig. 3 by HSE06 method and in Fig. S2 by GGA method. For HM ferromagnets, the spin-polarization at the Fermi level E_F must be 100 %, which is according to the following formula:

$$SP = \frac{N\uparrow(E_F) - N\downarrow(E_F)}{N\uparrow(E_F) + N\downarrow(E_F)} \quad (4)$$

where $N\uparrow(E_F)$ and $N\downarrow(E_F)$ correspond to the spin-up and spin-down densities of states at the Fermi level E_F . As can be seen from Fig. 3, the CsVF₂, CsVCl₂, CsVI₂ and CsCrI₂ alloys exhibit complete 100 % spin-polarization. The bandgap in one of the two spin channels and complete 100 % spin-polarization ensure the HM character of these alloys, while the remaining alloys are MSC by HSE06 method. In GGA calculations, for all eight alloys, the density of states in the spin-up channel crosses the Fermi level E_F , while the spin-down channel opens large bandgap as shown in Fig. S2. For CsVZ₂ ($Z = F$, Cl, Br or I) alloys, in both channels, the APDOS of the Cs atom is distributed at deep energy around -9 eV and those of the Z atoms are mainly distributed between -6.01 to -4.58 eV in CsVF₂ alloy, -5.45 to -3.61 eV in CsVCl₂ alloy, -5.13 to -2.99 to eV in CsVBr₂ alloy and -4.81 to -2.24 eV in CsVI₂ alloy. Similarly, for CsCrZ₂ ($Z = F$, Cl, Br or I) alloys, in both channels, the APDOS of the Cs atom is distributed around -8 eV and those of the Z atoms are mainly distributed between -5.08 to -3.75 eV in CsCrF₂ alloy, -4.66 to -2.88 eV in CsCrCl₂ alloy, -4.37 to -2.31 to eV in CsCrBr₂ alloy and -4.06 to -1.62 eV in CsCrI₂ alloy. The APDOS of both Cs and Z atoms do not show obvious spin-splitting, because after one 6 s electron of Cs atom and one 4 s electron of V (Cr) atom transfer to the p orbitals of two Z atoms, all occupied orbitals are completely filled for either Cs or Z atoms. The increasing in orbital radius for $Z = F$, Cl, Br or I successively lead the APDOS of the Z atoms not only broadening (more dispersion) but also shifting upwards to higher energy region. However, the large positive spin-splitting of about 2.3 eV (3.4 eV) is observed for V (Cr) atom, its spin-up channel is located around the Fermi level E_F , while its spin-down channel shifts upwards to around 2.3 eV (3.2 eV). These alloys are considered as ideal candidate materials for spintronic devices because of their excellent HM and MSC behavior.

Magnetic properties

In this section, we explore the magnetic properties of the CsYZ₂ ($Y = V$ or Cr; $Z = F$, Cl, Br or I) full-Heusler alloys. According to the valence electron structures of the Cs ($6s^1$), V ($3d^34s^2$), Cr ($3d^54s^1$), F ($2s^22p^5$), Cl ($3s^23p^5$), Br ($4s^24p^5$) and I ($5s^25p^5$), there are total of 20 valence electrons in CsVZ₂ ($Z = F$, Cl, Br or I) alloys and 21 in CsCrZ₂ ($Z = F$, Cl, Br or I) alloys. From the integrated TDOS, there are total of 12 spin-up and 8 spin-down electrons at the Fermi level E_F i.e. $N\uparrow = 12$ and $N\downarrow = 8$ in CsVZ₂ ($Z = F$, Cl, Br or I) alloys. Therefore, the total magnetic moments are $M_t = N\uparrow - N\downarrow = 12 - 8 = 4 \frac{\mu_B}{f.u.}$ Similarly, for the CsCrZ₂ ($Z = F$, Cl, Br or I) alloys, the $N\uparrow = 13$ and $N\downarrow = 8$, so $M_t = N\uparrow - N\downarrow = 13 - 8 = 5 \frac{\mu_B}{f.u.}$ satisfy the Slater-Pauling rule $M_t = N\uparrow - N\downarrow = (Z_t - N\downarrow) - N\downarrow = (Z_t - 2N\downarrow) = Z_t - 16$, where Z_t is the total number of valence electrons. To prove our statements, we calculated the integrated density of states IDOS (number of states NOS) of the CsVCl₂ and CsCrCl₂ full-Heusler alloys. We find that the spin-up channel of the CsVCl₂ (CsCrCl₂) alloys contains 12 (13) electrons while spin-down channel contains 8 (8) electrons, therefore total magnetic moment M_t per unit cell of the CsYZ₂ ($Y = V$ or Cr; $Z = F$, Cl, Br or I) alloys are 4.00 or 5.00 $\frac{\mu_B}{f.u.}$, also satisfy the Slater-Pauling rule $M_t = Z_t - 16$ as shown in Fig. S3.

In addition, according to valence electron structures, four valence electrons occupy s orbital of two Z atoms, twelve electrons occupy the p orbital of two Z atoms, and the remaining four (five) electrons occupy the spin-up states of V-3d (Cr-3d) orbitals, so as listed in Table S3, the total magnetic moments M_t per unit cell of 4.00 (5.00) $\frac{\mu_B}{f.u.}$ have been obtained for CsVZ₂ (CsCrZ₂) ($Z = F$, Cl, Br or I) full-Heusler alloys. While in CsVO₂ (CsCrO₂) full-Heusler alloys, the total magnetic moments M_t per unit cell are only 2.00 (3.00) $\frac{\mu_B}{f.u.}$. This is because in CsVO₂ (CsCrO₂), each Cs and each V (Cr) atom donate one and three valence electrons to two oxygen atoms and becoming positively ionized (+1) and (+3), respectively, the oxygen atom becomes negatively charged (-2) by receiving additional electrons as a nominal valence, i.e. $Cs^{+1}V^{+3}O_2^2$ ($Cs^{+1}Cr^{+3}O_2^2$). For these alloys, the Slater-Pauling rule is different from traditional Slater-Pauling rules $M_t = Z_t - 18$, $M_t = Z_t - 24$ or $M_t = Z_t - 28$ [47,48]. The atomic magnetic moment M_a of each atom in CsYZ₂ ($Y = V$ or Cr; $Z = F$, Cl, Br or I) full-Heusler alloys are listed in Table S3 along with those in CsYO₂ ($Y = V$ or Cr) alloys [24] for comparison. The main contribution of the total magnetic moment M_t comes from the V or Cr atoms while the atomic magnetic moment M_a of Cs and Z atoms is nearly zero due to their complete filled outermost shells. The V or Cr atoms have the largest magnetic moments due to the strong exchange splitting between the spin-up and spin-down states of their d electrons. From atomic IDOS, the Cs and Cl atoms have the same number of spin-up and spin-down electrons at the Fermi level while four (five) electrons occupy the spin-up states of V-3d (Cr-3d) orbitals as shown in Fig. S3. It is worth noting that the CsYZ₂ ($Y = V$ or Cr; $Z = F$, Cl, Br or I) alloys are all HM ferromagnets by GGA method.

For alloys composed of transition metal elements, the Coulomb force between d-d electrons has a great influence on the electronic and magnetic properties. The alloys considered in this study contain transition metals, so it is necessary to study the effect of electron localization on the electronic states. To exemplify this problem, GGA + U [49] has been used to calculate Hubbard-type Coulomb interaction. Fig. S4 shows the TDOS of the CsYZ₂ ($Y = V$ or Cr; $Z = F$, Cl, Br or I) full-Heusler alloys with GGA + U ($U = 1.00$, 2.00 or 3.00 eV) for 3d orbitals of V or Cr elements. It could be seen that all the alloys are still HM materials with U changes from 1.00 to 3.00 eV for Y-3d electrons. Similarly, the total magnetic moments M_t ($\frac{\mu_B}{f.u.}$) and atomic magnetic moments M_a ($\frac{\mu_B}{atom}$), of the CsYZ₂ ($Y = V$ or Cr; $Z = F$, Cl, Br or I) full-Heusler alloys by GGA + U method with $U = 1.00$, 2.00 or 3.00 eV for $Y = V$ or Cr-3d electrons are given in Table S5. Our results show that the Coulomb interaction has no significant effect on the magnetic moment of these alloys. This phenomenon indicates that the HM character of CsYZ₂ ($Y = V$ or Cr; $Z = F$,

Cl, Br or I) full-Heusler alloys remains the same when Coulomb interaction is considered.

Mechanical properties

The elastic constants provide information about mechanical stability, dynamic stability, bonding nature, stiffness and ductility of the materials. In order to determine the elastic constants (C_{ij}) and mechanical stability, first, we determine the elastic constants, which are important parameters and can be investigated by the stress-strain method [50,51]. The number of elastic constants depends on the symmetry of the crystal structure. The cubic system has only three independent elastic constants C_{11} , C_{12} , and C_{44} [52,53]. The elastic constants C_{11} is related to the material elasticity in length while C_{12} and C_{44} are related to the elasticity in shape.

The elastic constants C_{ij} and stability conditions of the CsYZ_2 ($Y = \text{V}$ or Cr ; $Z = \text{F}$, Cl , Br or I) full-Heusler alloys at different pressures P (GPa) are shown in Fig. S5. The Born's mechanical stability conditions under different pressures are given by the following formulas [54,55]:

$$\begin{cases} C_{44}-P > 0 \\ C_{11}-C_{12}-2P > 0 \\ C_{11}+2C_{12}+P > 0 \end{cases} \quad (5)$$

As is clear from Fig. S5, for the CsYZ_2 ($Y = \text{V}$ or Cr ; $Z = \text{F}$, Cl , Br or I) full-Heusler alloys, C_{11} , C_{12} , and C_{44} increase with increasing pressure. These alloys lose their mechanical stability when the pressure exceeds 20 GPa (25 GPa) for $Y = \text{V}$ (Cr).

Optical properties

The optical properties of materials are crucial for understanding how they interact with light. One fundamental parameter that characterizes these properties is the absorption coefficient $\alpha(\omega)$, which quantifies how much a material can absorb incident light. Materials with low absorption coefficients absorb minimal light, indicating their transparency to a

broader range of wavelengths. The absorption coefficient is pivotal in determining the light penetration depth within a material, shedding light on how far light can travel before being absorbed. In this context, we explore the optical properties of CsYZ_2 ($Y = \text{V}$ or Cr ; $Z = \text{F}$, Cl , Br , or I) full-Heusler alloys by HSE06 method in Fig. 4 (a), focusing on their absorption coefficients $\alpha(\omega)$ with photon energy which is represented by the following relationship:

$$\alpha(\omega) = \frac{4k\pi}{\lambda} = \frac{\omega}{nc} \epsilon_2(\omega) \quad (6)$$

Our results show that the absorption coefficient $\alpha(\omega)$ of the CsVF_2 alloy is better in the visible region.

Reflectivity is another crucial optical property, defined as the reflection of light from a material's surface. The reflectivity index $R(\omega)$ measures how much incident light is reflected as a function of photon energy. It offers insights into how efficiently a material reflects light at different energy levels. In Fig. 4 (b), the reflectivity index $R(\omega)$ curves are plotted for the CsYZ_2 ($Y = \text{V}$ or Cr ; $Z = \text{F}$, Cl , Br or I) full-Heusler alloys, revealing their response to incident light. The reflectivity index $R(\omega)$ curves as a function of photon energy is defined as follows:

$$R(\omega) = \left| \frac{\epsilon_1(\omega) + i\epsilon_2(\omega)^{1/2} - 1}{\epsilon_1(\omega) + i\epsilon_2(\omega)^{1/2} + 1} \right| \quad (7)$$

The reflectivity index $R(\omega)$ curves indicate that the reflectivity index $R(\omega)$ of the CsVB_2 and CsVI_2 alloys are better in the visible region. It is worth noting that the highest peaks of the absorption coefficient $\alpha(\omega)$ and reflectivity index $R(\omega)$ are located in the UV region. For comparison, the absorption coefficient $\alpha(\omega)$ and reflectivity index $R(\omega)$ of the CsYZ_2 ($Y = \text{V}$ or Cr ; $Z = \text{F}$, Cl , Br or I) full-Heusler alloys using GGA method is also given in Fig. S6.

Thermoelectric properties

It is a well accepted fact that a major part of the fuel used either in

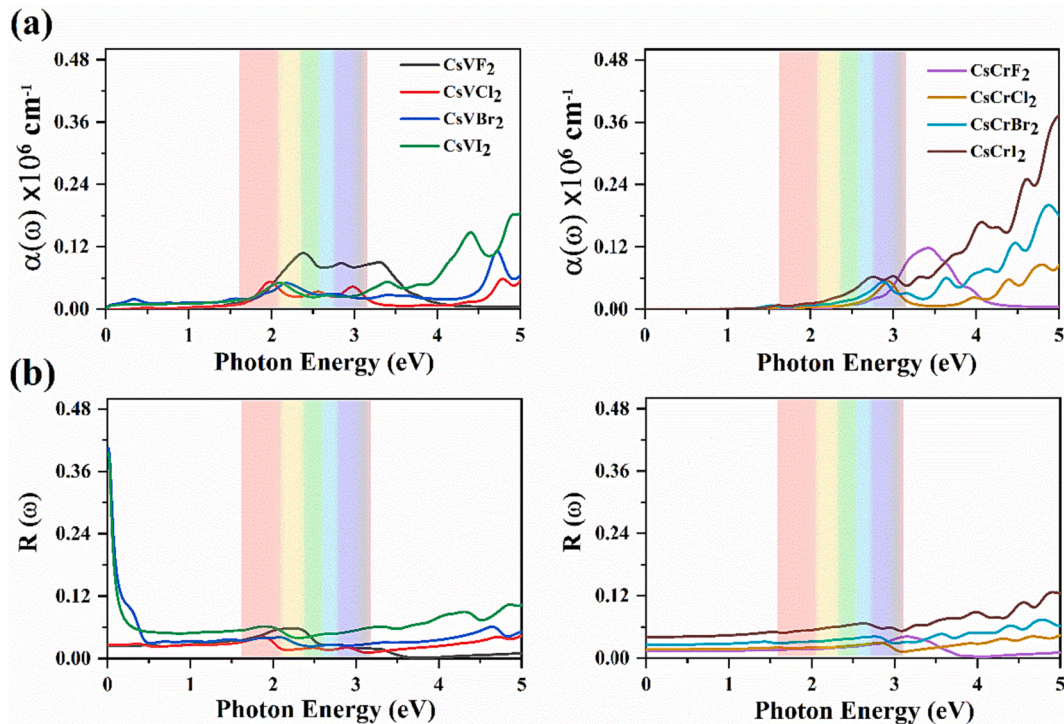


Fig. 4. The absorption coefficient $\alpha(\omega)$ and reflectivity index $R(\omega)$ as a function of photon energy for the CsYZ_2 ($Y = \text{V}$ or Cr ; $Z = \text{F}$, Cl , Br or I) full-Heusler alloys using HSE06 method.

vehicles or industries is lost as heat, causing increased fuel consumption. In order to overcome this issue and convert the waste heat into useful energy such as electrical energy, thermoelectric (TE) materials have drawn particular attention in the research community [56–58]. Additionally, these materials can also be useful in converting solar energy into electricity, providing another opportunity for producing the fuel useful energy. Moreover, TE devices have superior advantages including environmentally friendly energy conversion with no pollutants and feasibility over a wide temperatures range [59].

Following the early research work on the TE properties of semiconductor Bi_2Te_3 , extensive efforts have been carried out in finding the high performance TE materials [60,61]. In this study, to explore new TE materials, we investigated the TE properties of CsYZ_2 ($\text{Y} = \text{V}$ or Cr ; $\text{Z} = \text{F}$, Cl , Br or I) full-Heusler alloys using BoltzTrap code using HSE06 method. To comprehensively understand TE behavior, the various related parameters including electronic thermal conductivity κ_e/τ , electrical conductivity σ/τ , and Seebeck coefficient S of the present materials are calculated as a function of chemical potential (μ) at temperature of 300, 500 and 700 K, shown in Figs. 5–8, respectively. In solids, heat transportation is mainly carried by electrons and phonons (lattice-part). In our case, only the electronic part is considered as the code in its present form is not able to calculate the lattice thermal conductivity. Second important point is that all calculations are performed by assuming a constant relaxation time τ . Therefore, our study provides a reference for the future work.

Firstly, we discuss the Seebeck coefficient S shown in Fig. 5. In fact, S itself is related with the temperature gradient between the two ends of the conducting material. A voltage called Seebeck-voltage is induced when a net flow of electrons takes places between the two points at different temperature. Note that, depending on the nature of charge carriers responsible for transport, S may have positive or negative value, but the materials with large S are preferred for TE applications. In general, a positive (negative) value of S refers to a p-type (n-type) nature of the material. From Fig. 5, it is obvious that in CsV -based compounds S is initially negative around $\mu=-1.0$ eV, then with increasing μ the S becomes positive and reaches a maximum value. Afterwards, S decreases and becomes negative at Fermi level. It means at Fermi level the majority charge carriers are electrons which contribute to heat transport.

Among CsCr -based compounds, all materials except for $\text{X} = \text{I}$, have somewhat symmetric S above and below Fermi level. These materials have achieved a maximum S value for $\mu = -0.50$ to 0 eV. Furthermore, below Fermi level, the positive charge carriers have a dominant contribution to the heat transport. The different trend in S variation for $\text{X} = \text{I}$ might be attributed to the different electronic band structure of this compound, which is expected to be responsible for the observed trend in S . Among all eight materials, the maximum S reaches 1500 $\mu\text{V/K}$.

The electrical conductivity $(\sigma/\tau)d$ is shown in Fig. 6 reveals some interesting features. For example, electrical conductivity is almost independent of temperature as all plots are identical. For $\text{X} = \text{F}$, Cl , Br the electrical conductivity increases with chemical potential, then it reaches a minimum level at Fermi level. For positive chemical potential, the electrical conductivity continuously increases. In CsCrF_2 , CsCrCl_2 and CsCrBr_2 , the electrical conductivity is almost zero around Fermi level. The electrical conductivity of CsCrI_2 has a maximum value of about 4×10^{19} in standard units.

The electronic thermal conductivity (κ_e/τ) is presented in Fig. 7. Clearly, for majority of materials, temperature has a significant effect on the κ_e/τ . In particular, κ_e/τ for CsVI_2 is more sensitive and increases obviously with temperature. The total thermal conductivity κ is $\kappa = \kappa_e + \kappa_l$ is the sum of electronic and lattice thermal conductivity [62]. For better thermoelectric performance, materials with low lattice thermal conductivity and high electronic thermal conductivity are regarded as suitable ones. The efficiency of a thermoelectric device is measured in terms of unit-less figure of merit written as ZT and given by $\text{ZT} = (S^2 \sigma T)/\kappa$, where T is the operating temperature of the device [61]. The calculated ZT is shown in Fig. 8. Obviously, for high ZT, the material should have large S and σ , and low κ . The maximum $\text{ZT} = 0.7$ is obtained for CsCrBr_2 , while, lowest $\text{ZT} = 0.3$ is for CsVI_2 . Other investigated materials have ZT between 0.3 and 0.7. These results demonstrate that the ZT value can be tuned by varying the chemical composition of the present materials.

Conclusions

We investigate the structural, electronic, magnetic, mechanical, optical and thermoelectric properties of full-Heusler alloys CsYZ_2 ($\text{Y} = \text{V}$ or

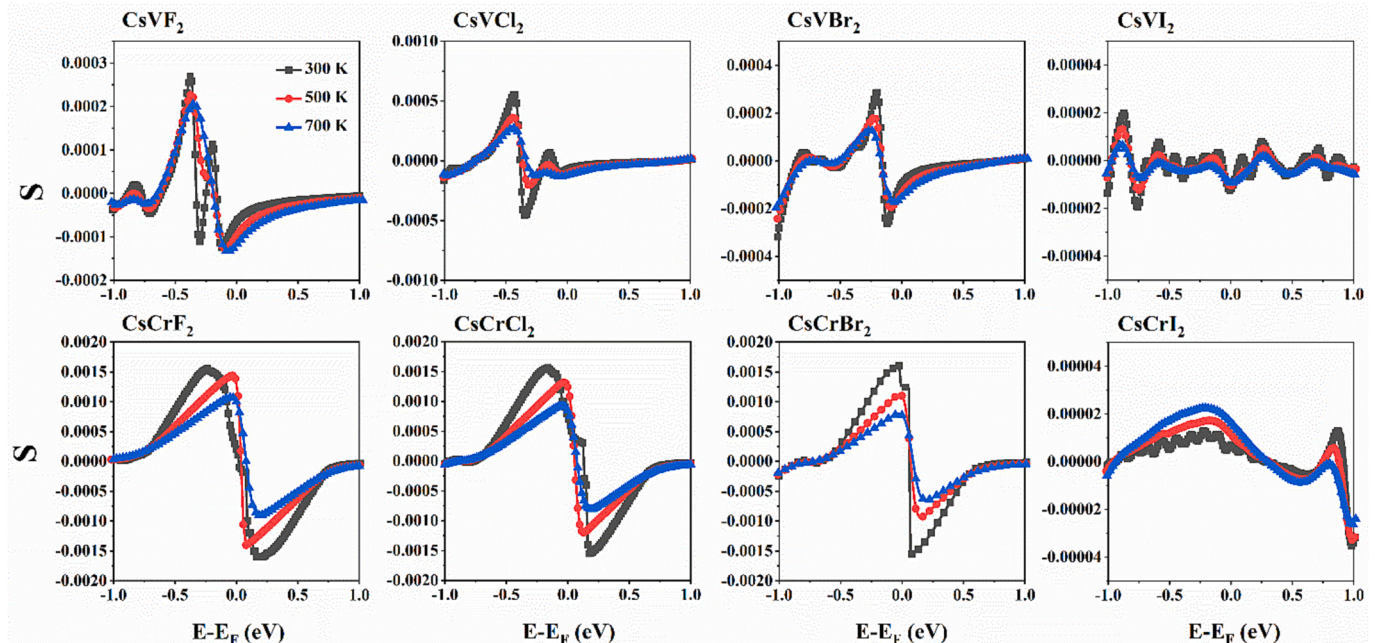


Fig. 5. The Seebeck coefficient (S) as a function of the chemical potential at different temperatures for CsYZ_2 ($\text{Y} = \text{V}$ or Cr ; $\text{Z} = \text{F}$, Cl , Br or I) full-Heusler alloys using HSE06 method.

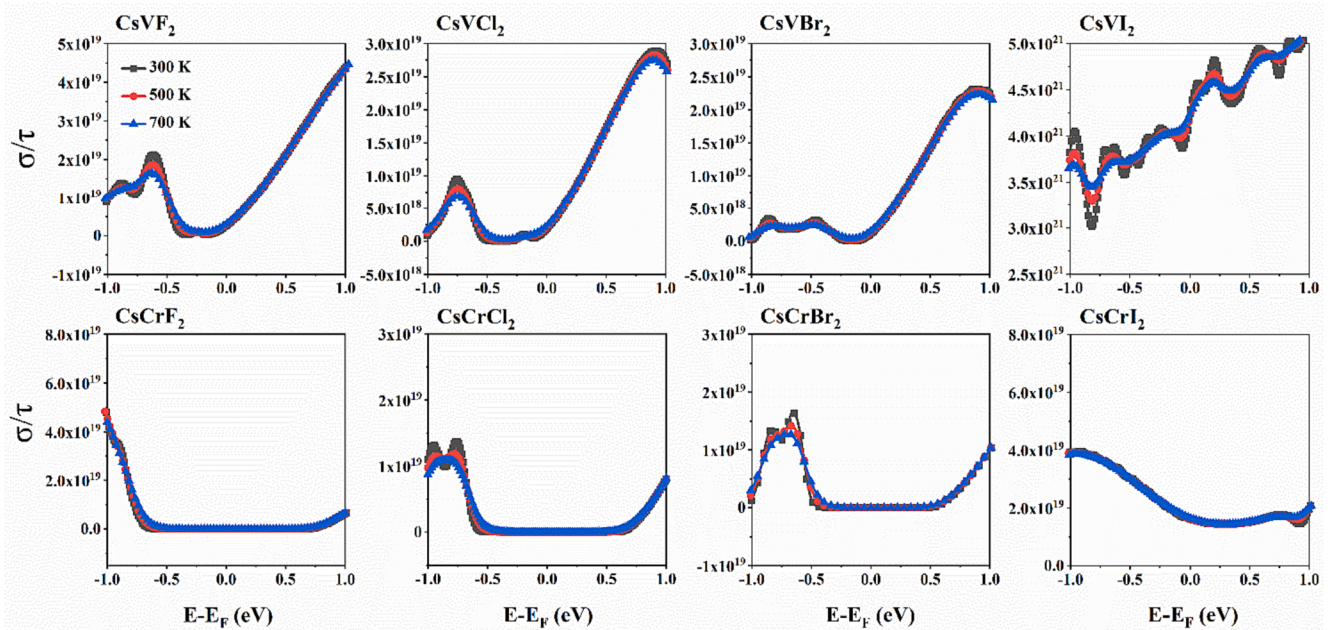


Fig. 6. The electrical conductivity σ/τ as a function of the chemical potential at different temperatures for CsYZ_2 ($Y = \text{V}$ or Cr ; $Z = \text{F}$, Cl , Br or I) full-Heusler alloys using HSE06 method.

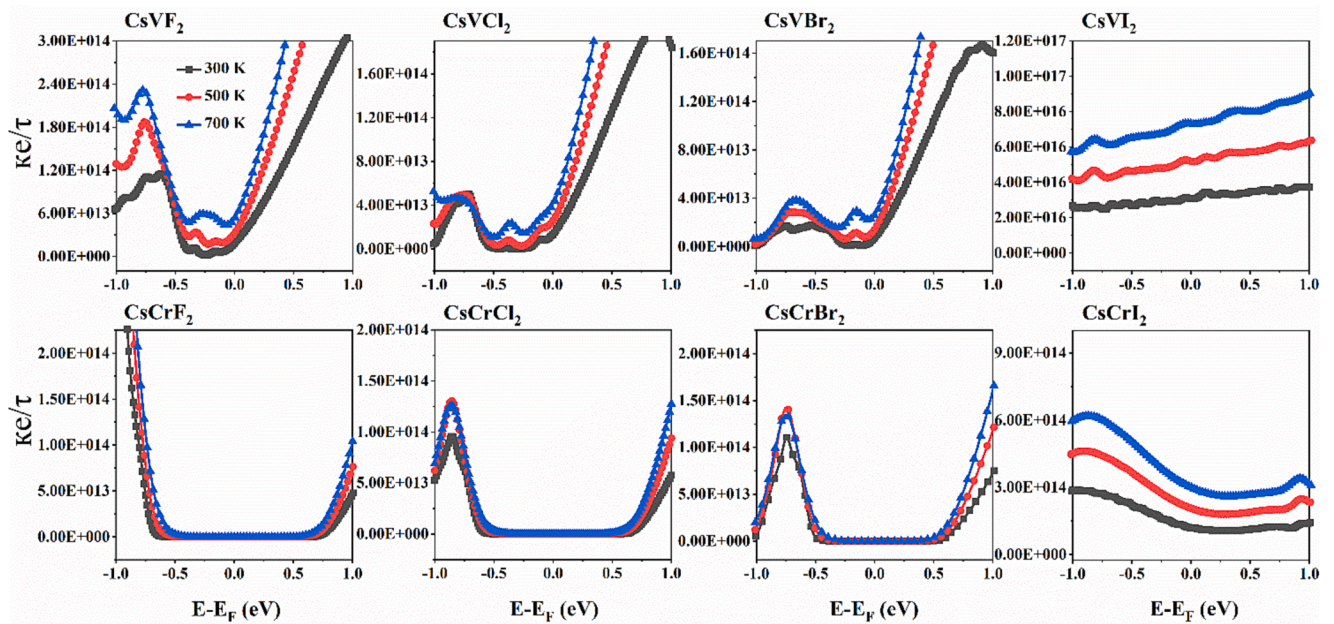


Fig. 7. The electronic thermal conductivity κ_e/τ as a function of the chemical potential at different temperatures for CsYZ_2 ($Y = \text{V}$ or Cr ; $Z = \text{F}$, Cl , Br or I) full-Heusler alloys using HSE06 method.

Cr ; $Z = \text{F}$, Cl , Br or I) by using first-principles calculations within GGA and HSE06 methods. The main conclusions are listed as follows:

1. The large absolute values of both cohesive and formation energies indicate their thermodynamic stability.
2. The CsYZ_2 ($Y = \text{V}$ or Cr ; $Z = \text{F}$, Cl , Br or I) alloys exhibit very large total magnetic moment M_t of 4.00 or $5.00 \frac{\mu_B}{\text{f.u.}}$, respectively, following the Slater-Pauling rule $M_t = Z_t \cdot 16$.
3. The CsVF_2 , CsVCl_2 , CsVI_2 and CsCrI_2 alloys are all HM ferromagnets while remaining alloys exhibits MSC behavior.
4. The absorption coefficient $\alpha(\omega)$ of the CsVF_2 alloy is better in the visible region.

5. These alloys are considered as ideal candidates for spintronics and magnetoelectronics applications.

CRediT authorship contribution statement

Iltaf Muhammad: Writing – original draft, Formal analysis, Data curation, Conceptualization. **Shehzad Ahmed:** Formal analysis. **Naeem Ullah:** Resources, Funding acquisition. **Muhammad Mushtaq:** Writing – review & editing. **Maryam Liaqat:** Formal analysis, Validation, Visualization, Writing – review & editing. **Xiaoqing Tian:** Supervision, Software, Resources, Investigation. **Jian-Min Zhang:** Methodology, Investigation, Data curation, Conceptualization.

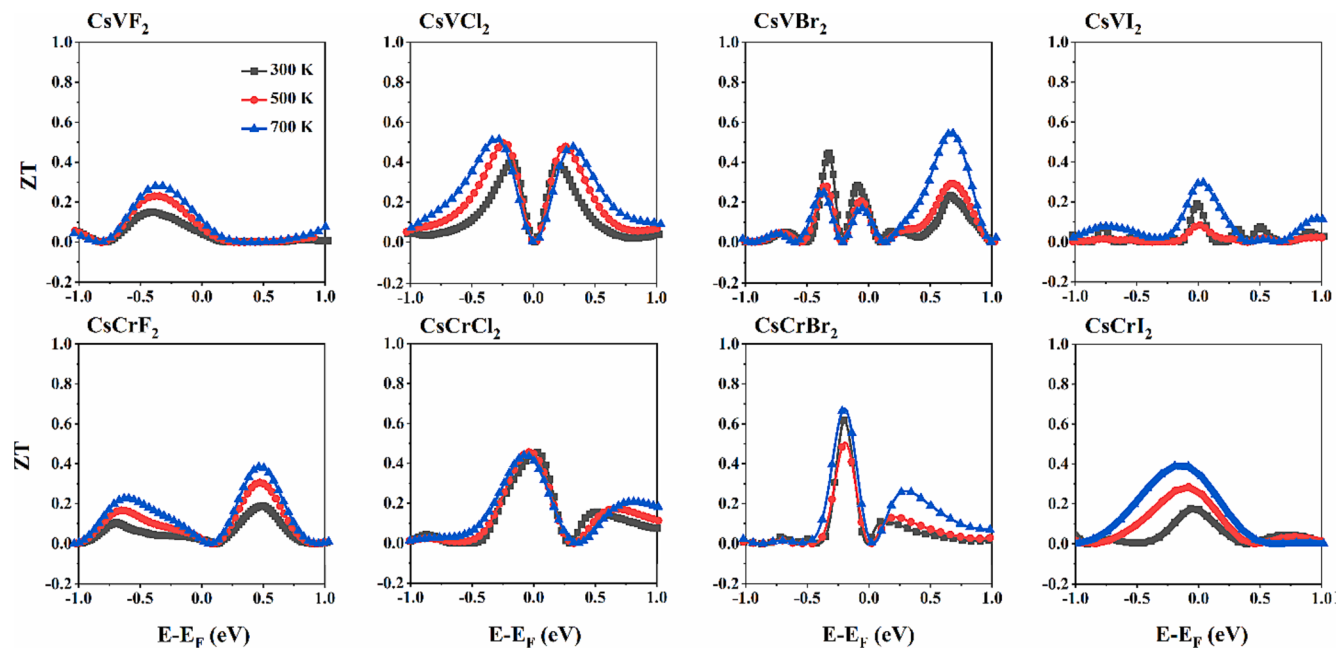


Fig. 8. The figure of merit (ZT) as a function of the chemical potential at different temperatures for CsYZ_2 ($\text{Y} = \text{V}$ or Cr ; $\text{Z} = \text{F}$, Cl , Br or I) full-Heusler alloys using HSE06 method.

Declaration of competing interest

The authors declare that they have no known competing financial interests or personal relationships that could have appeared to influence the work reported in this paper.

Data availability

Data will be made available on request.

Acknowledgements

This work was supported by the Guangdong Basic and Applied Basic Research Foundation (2021A1515010082), Shenzhen Fundamental Research Program (JCYJ20190808121405740) and the National Natural Science Foundation of China (62250410369).

Appendix A. Supplementary data

Supplementary data to this article can be found online at <https://doi.org/10.1016/j.rinp.2024.107419>.

References

- [1] Prinz GA. Spin-polarized transport. *Phys Today* 1995;48:58–63.
- [2] Magnetoelectronics PGA. *Science* (80-) 1998;282:1660–3.
- [3] Inomata K, Ikeda N, Tezuka N, Goto R, Sugimoto S, Wojcik M, et al. Highly spin-polarized materials and devices for spintronics(*). *Sci Technol Adv Mater* 2008;9: 14101.
- [4] Liu W, Wong PKJ, Xu Y. Hybrid spintronic materials: Growth, structure and properties. *Prog Mater Sci* 2019;99:27–105.
- [5] Heusler F, Starck W, Haupt E. *Magnetisch-Chemische Studien Verh Dtsch Phys Ges* 1903;5:219–32.
- [6] de Groot RA, Mueller FM, van Engen PG, Buschow KJH. New Class of Materials: Half-Metallic Ferromagnets. *Phys Rev Lett* 1983;50:2024–7.
- [7] Galanakis I, Dederichs PH. *Half-Metallic Alloys: Fundamentals and Applications*, vol. 676. Springer; 2005.
- [8] Tobola J, Pierre J. Electronic phase diagram of the XTZ ($\text{X} = \text{Fe}, \text{Co}, \text{Ni}; \text{T} = \text{Ti}, \text{V}, \text{Zr}, \text{Nb}, \text{Mn}; \text{Z} = \text{Sn}, \text{Sb}$) semi-Heusler compounds. *J Alloys Compd* 2000;296:243–52.
- [9] Kojima T, Kameoka S, Fujii S, Ueda S, Tsai A-P. Catalysis-tunable Heusler alloys in selective hydrogenation of alkynes: A new potential for old materials. *Sci Adv* 2018;4: eaat6063.
- [10] Li S, Zhao H, Li D, Jin S, Gu L. Synthesis and thermoelectric properties of half-Heusler alloy YNiBi . *J Appl Phys* 2015;117.
- [11] Muhammad I, Zhang J-M, Ali A, Muhammad S. Preserving the half-metallicity at the quaternary Heusler CoFeCrAl (001)-oriented thin films: A first-principles study. *Mater Chem Phys* 2020;240:122262.
- [12] Khandy SA, Kaur K, Dhiman S, Singh J, Kumar V. Exploring thermoelectric properties and stability of half-Heusler PtXSn ($\text{X} = \text{Zr}, \text{Hf}$) semiconductors: A first principle investigation. *Comput Mater Sci* 2021;188:110232.
- [13] Khandy SA, Chai JD. Thermoelectric properties, phonon, and mechanical stability of new half-metallic quaternary Heusler alloys: FeRhCrZ ($\text{Z} = \text{Si}$ and Ge). *J Appl Phys* 2020;127.
- [14] Galanakis I, Dederichs PH, Papanikolaou N. Origin and properties of the gap in the half-ferromagnetic Heusler alloys. *Phys Rev B* 2002;66:134428.
- [15] Khandy SA. Inspecting the electronic structure and thermoelectric power factor of novel p-type half-Heuslers. *Sci Rep* 2021;11:1–10.
- [16] Khandy SA, Da CJ. Origin of pseudo gap and thermoelectric signatures of semimetallic Ru_2TaGa : Structural stability from phonon dynamics, mechanical, and thermodynamic predictions. *J Phys Chem Solids* 2021;154:110098.
- [17] Khandy SA, Da CJ. Strain engineering of electronic structure, phonon, and thermoelectric properties of p-type half-Heusler semiconductor. *J Alloys Compd* 2021;850:156615.
- [18] Khandy SA, Islam I, Kaur K, Ali AM, Abd El-Rehim AF. Effect of Strain on the Electronic Structure and Phonon Stability of SrBaSn Half Heusler Alloy. *Molecules* 2022;27:3785.
- [19] Bainsla L, Suresh KG. Equiatomic quaternary Heusler alloys: A material perspective for spintronic applications. *Appl Phys Rev* 2016;3(3):031101.
- [20] Ozdog K, Galanakis I. First-principles electronic and magnetic properties of the half-metallic antiferromagnet Cr_2MnSb . *J Magn Magn Mater* 2009;321:L34–6.
- [21] Song J-T, Zhang J-M. The structural, electronic, magnetic and elastic properties of the binary Heusler alloys Mn_2Z ($\text{Z} = \text{As}, \text{Sb}, \text{Bi}$): a first-principles study. *Mater Res Express* 2017;4:116501.
- [22] Song J-T, Zhang J-M. The structural, electronic, magnetic and optical properties of the half-metallic binary alloys ZCl_3 ($\text{Z} = \text{Be}, \text{Mg}, \text{Ca}, \text{Sr}$): a first-principles study. *Superlattices Microstruct* 2018;118:230–41.
- [23] Fan L, Chen F, Li C, Hou X, Zhu X, Luo J, et al. Promising spintronics: Mn-based Heusler alloys Mn_3Ga , Mn_2YGa ($\text{Y} = \text{V}, \text{Nb}, \text{Ta}$). *ScMnVGa* *J Magn Magn Mater* 2020;497:166060.
- [24] Fan L, Chen F, Chen Z-Q. First-principles calculations of magnetism and half-metallic properties of CsYO_2 ($\text{Y} = \text{V}, \text{Cr}, \text{Mn}, \text{Fe Co, Ni}$) Heusler alloys. *J Magn Magn Mater* 2019;478:264–73.
- [25] Wang X, Cheng Z, Liu G. Largest magnetic moments in the half-Heusler alloys XCrZ ($\text{X} = \text{Li}, \text{K}, \text{Rb}, \text{Cs}; \text{Z} = \text{S}, \text{Se}, \text{Te}$): A first-principles study. *Materials (basel)* 2017;10: 1078.
- [26] Cherid S, Benstaali W, Abbad A, Bentata S, Lantri T, Abbar B. Theoretical prediction of half metallic ferromagnetic full-Heusler alloys Cs_2CrGe . *Solid State Commun* 2017;260:14–8.
- [27] Damewood L, Busemeyer B, Shaughnessy M, Fong CY, Yang LH, Felser C. Stabilizing and increasing the magnetic moment of half-metals: The role of Li in half-Heusler LiMnZ ($\text{Z} = \text{N}, \text{P}, \text{Si}$). *Phys Rev B* 2015;91:64409.
- [28] Difaf M, Righi H, Rached H, Rached D, Beddraf R. Ab Initio Study of the Properties of $\text{Ti}_2\text{PdFe}(\text{Ru})\text{Sb}_2$ Double Half-Heusler Semiconducting Alloys. *J Electron Mater* 2023;52:6514–29.

- [29] Rached D, Boumia L, Caid M, Rached Y, Ait Belkacem AA, Rached H, et al. The half-metallic ferromagnetic and thermoelectric responses of the potential thermo-spintronic compounds CrTiRhZ (Z: Al or Si) QHA. *Indian J Phys* 2023;.
- [30] Bourachid I, Caid M, Rached Y, Rached D, Bouafia H, Abidri B, et al. Theoretical insight into the stability, magneto-electronic and thermoelectric properties of V₂MnAs Heusler alloy. *Indian J Phys* 2023;.
- [31] Rached Y, Rached D, Rached H, Cheref O, Caid M, Merabet M, et al. DFT assessment on stabilities, electronic and thermal transport properties of Co_xZrSb_{1-x}Bix half-Heusler alloys and their superlattices. *Eur Phys J plus* 2023;138:307.
- [32] Youcef A, Bettahar N, Cheref O, Benalia SE, Rached D, Benkhetou NE, et al. Topologically nontrivial phase in Na₂CuX (X= As, Sb, Sn and Bi) full Heusler compounds: Insights from DFT-based computer simulation. *Rev Mex Fis* 2023;69:1–8.
- [33] Bourachid I, Rached D, Rached H, Bentouaf A, Rached Y, Caid M, et al. Magneto-electronic and thermoelectric properties of V-based Heusler in ferrimagnetic phase. *Appl Phys A Mater Sci Process* 2022;128:1–13.
- [34] Rached Y, Caid M, Rached H, Merabet M, Benalia S, Al-Qaisi S, et al. Theoretical Insight into the Stability, Magneto-electronic and Thermoelectric Properties of XC_xSb (X: Fe, Ni) Half-Heusler Alloys and Their Superlattices. *J Supercond Nov Magn* 2022;35:875–87.
- [35] Kresse G, Hafner J. Ab initio molecular dynamics for liquid metals. *Phys Rev B* 1993;47:558.
- [36] Kresse G, Hafner J. Ab initio molecular-dynamics simulation of the liquid-metal-amorphous-semiconductor transition in germanium. *Phys Rev B Condens Matter* 1994;49:14251–69.
- [37] Kresse G, Furthmüller J. Efficiency of ab-initio total energy calculations for metals and semiconductors using a plane-wave basis set. *Comput Mater Sci* 1996;6:15–50.
- [38] Kresse G, Furthmüller J. Efficient iterative schemes for ab initio total-energy calculations using a plane-wave basis set. *Phys Rev B* 1996;54:11169–86.
- [39] Kresse G, Joubert D. From ultrasoft pseudopotentials to the projector augmented-wave method. *Phys Rev B* 1999;59:1758–75.
- [40] Perdew JP, Burke K, Ernzerhof M. Generalized Gradient Approximation Made Simple. *Phys Rev Lett* 1996;77:3865–8.
- [41] Paier J, Marsman M, Hummer K, Kresse G, Gerber IC, Ángyán JG. Screened hybrid density functionals applied to solids. *J Chem Phys* 2006;124:154709.
- [42] Clementi E, Raimondi D-L. Atomic screening constants from SCF functions. *J Chem Phys* 1963;38:2686–9.
- [43] Allred AL. Electronegativity values from thermochemical data. *J Inorg Nucl Chem* 1961;17:215–21.
- [44] Wei X-P, Chu Y-D, Sun X-W, Deng J-B. First-principles study on stability, electronic and thermodynamic properties of Ti₂CoIn and Ti₂NiIn. *Eur Phys J B* 2013;86:1–7.
- [45] Kurz P, Bihlmayer G, Blügel S. Magnetism and electronic structure of hcp Gd and the Gd (0001) surface. *J Phys Condens Matter* 2002;14:6353.
- [46] Siakeng L, Mikhailov GM, Rai DP. Electronic, elastic and X-ray spectroscopic properties of direct and inverse full Heusler compounds Co₂FeAl and Fe₂CoAl, promising materials for spintronic applications: a DFT+ U approach. *J Mater Chem C* 2018;6:10341–9.
- [47] Galanakis I, Dederichs PH, Papanikolaou N. Slater-Pauling behavior and origin of the half-metallicity of the full-Heusler alloys. *Phys Rev B* 2002;66.
- [48] Skafiotouros S, Özdogan K, Şaşoğlu E, Galanakis I. Generalized Slater-Pauling rule for the inverse Heusler compounds. *Phys Rev B* 2013;87:24420.
- [49] Dudarev SL, Botton GA, Savrasov SY, Humphreys CJ, Sutton AP. Electron-energy-loss spectra and the structural stability of nickel oxide: An LSDA+U study. *Phys Rev B* 1998;57:1505–9.
- [50] Ponce CA, Casali RA, Caravaca MA. Ab initio study of mechanical and thermo-acoustic properties of tough ceramics: applications to HfO₂ in its cubic and orthorhombic phase. *J Phys Condens Matter* 2008;20:45213.
- [51] Le Page Y, Saxe P. Symmetry-general least-squares extraction of elastic coefficients from ab initio total energy calculations. *Phys Rev B* 2001;63:174103.
- [52] Mouhat F, Couder F-X. Necessary and sufficient elastic stability conditions in various crystal systems. *Phys Rev B* 2014;90:224104.
- [53] Shafiq M, Arif S, Ahmad I, Asadabadi SJ, Maqbool M, Aliabad HAR. Elastic and mechanical properties of lanthanide monoxides. *J Alloys Compd* 2015;618:292–8.
- [54] Zhou Z, Joós B. Stability criteria for homogeneously stressed materials and the calculation of elastic constants. *Phys Rev B* 1996;54:3841.
- [55] Liu M, Cheng Y, Yuan J-N, Ji G-F, Gong M. Elastic and electronic properties of LiBSi₂ under pressure from first principles. *Comput Mater Sci* 2014;92:231–7.
- [56] Kanatzidis MG. Nanostructured thermoelectrics: The new paradigm? *Chem Mater* 2010;22:648–59.
- [57] Yang L, Chen Z, Dargusch MS, Zou J. High performance thermoelectric materials: progress and their applications. *Adv Energy Mater* 2018;8:1701797.
- [58] Shen Z-G, Tian L-L, Liu X. Automotive exhaust thermoelectric generators: Current status, challenges and future prospects. *Energy Convers Manag* 2019;195:1138–73.
- [59] Winkler J, Aute V, Yang B, Radermacher R. Potential benefits of thermoelectric element used with air-cooled heat exchangers 2006.
- [60] Goldsmid HJ. The electrical conductivity and thermoelectric power of bismuth telluride. *Proc Phys Soc* 1958;71:633.
- [61] Zhang X, Zhao L-D. Thermoelectric materials: Energy conversion between heat and electricity. *J Mater* 2015;1:92–105.
- [62] Snyder GJ, Toberer ES. Complex thermoelectric materials. *Nat Mater* 2008;7:105–14.